Microstructural evolution of SiC powder in molten silicon

Jérôme Roger, Y. Le Petitcorps

Microstructural evolution of SiC powder in molten silicon

J. Roger [a,*], Y. Le Petitcorps[a]

[a] Université de Bordeaux, CNRS, Laboratoire des Composites ThermoStructuraux, UMR 5801, 33600 Pessac, France

* Corresponding author: e-mail: jerome.roger@lcts.u-bordeaux.fr

Abstract

SiC_{powder}/Si_{matrix} composites represent a new class of microstructurally toughened materials. The interactions between molten silicon and submicronic SiC powder have been considered since it could originate some limitations on the final properties of the material. Experiments putting in interaction a SiC powder and molten Si were performed while heating up to final values ranging between 1450 and 1600°C for duration up to 8 hours. The volume ratio of SiC and silicon was equal to one and SiC particles were freely dispersed within the liquid. X-ray diffraction analyses demonstrated that the apparent crystallites size increase of SiC powder followed a ripening law corresponding to a limitation either by volume diffusion or by dissolution into the liquid. Depending on the relevant mechanism, the activation energy of the crystallites' growth has been found equal to 357±50 $kJ.mol^{-1}$ or 441±57 $kJ.mol^{-1}$. An agglomeration-coarsening process of SiC particles was also identified which promoted a quick formation of larger particles.

Keywords: A Grain growth; B Composites; B Microstructure-final; B X-ray methods ;D SiC; E Structural applications;

1. Introduction

SiC compound has a great importance in a broad range of applications because of its very attractive properties: wide band gap, good oxidation resistance, high thermal stability and conductivity, low density and strong toughness. However, to obtain the best performances, the chemical behavior of this compound must be understood while it is synthetized and used. Many studies deal with the synthesis of SiC-based materials by a wide range of processes [1-10]. On the basis of these previous studies, one has to focus attention on the interactions between a liquid phase and SiC because they could have some influences on the resulting properties. The microstructure transformations observed during the interaction between a liquid metal and a ceramic were especially discussed by W.E. Lee et al. [11]. It was thus demonstrated that the presence of a low quantity of liquid during the SiC sintering at 1970°C for 6 hours was able to control the grain growth kinetic and the microstructure during the dissolution-precipitation transformation of β-SiC to α-SiC by generating a core/rim microstructure [12]. Several recent studies have also evidenced dissolution-precipitation processes during the infiltration of molten silicon into B_4C-based materials [13-15]. Moreover, the study reported by Y.W. Kim et al. relative to the β-SiC grain growth at 1800°C in presence of an oxynitride liquid suggested that the dissolution-growth mechanism is controlled by the diffusion of the species in the liquid [16]. Another study revealed that the grain growth of SiC particles in the presence of molten Si depends on the initial grain size [9]. Indeed, the authors found that the reactive sintering at 1600°C for 2 hours in argon of a α-SiC powder with an initial 0.2 µm size led to a final grain size up to 4.0 µm. Such a phenomenon was not observed by the authors in similar conditions except a starting powder exhibiting a mean grain size of 23.65 µm. This can be explained by the highest surface of contact between the liquid and the SiC powder with the finer grain size, which promotes the grain growth [17-20]. The study about α-SiC coarsening during sintering at 1950°C in presence of a liquid phase was realized by Sigl and Kleebe by addition of yttrium aluminum garnet (YAG) [21]. It was showed that coarsening occurs primarily by a solution-precipitation process, called

Ostwald ripening, with the growth of the larger grains at the expense of the smaller ones. H. Ye et al. also examined the coarsening of α-SiC during YAG-liquid phase sintering [22]. Their results also suggested that Ostwald ripening controls the sintering mechanism. Yet, the sintering of SiC materials actually implies a high temperature of heating close to 2000°C with an obvious grain growth [21-23]. The use of nanometric SiC powders is expected to considerably reduce the temperature, the time, the quantity of additives and to improve the properties of the final materials by promoting a very fine and dense microstructure [24-26]. Nevertheless, the sintering of such a pure powder remains laborious and requires high pressure, elevated temperature and more or less important quantities of additives [27-29]. In a recent study, X. Zhou et al. demonstrate the benefit of using silicon as sintering additive for a nano-scaled SiC powder to produce pure and dense ceramic [30]. Prior to the sintering, the authors have chemically treated the surface of the SiC grains in order to generate a carbonized layer able to consume silicon during the sintering and to produce a pure SiC material with promising properties. H. Schmidt et al. have succeeded in producing nano-sized SiC particles with diameter between 2 et 7 nm by precipitation in a Si-B-C-N amorphous matrix without liquid phase [31]. The SiC particles size rises up to 40 nm by a coarsening mechanism controlled by the diffusion in the matrix with an activation energy of 770 $kJ.mol^{-1}$. This value has to be compared to the ones of pure SiC nanograin growth which were reported to be in a range of 430 to 1060 $kJ.mol^{-1}$ depending on the densification mechanism [32]. In this way, the chemical interaction between molten silicon and a submicronic SiC powder is reported in the present paper. As, it is of importance to identify the effect of molten silicon on SiC transformations. Although SiC_{powder}/Si matrix composites represents a new class of potentially important structural materials, the evolution occurring during the silicon melt infiltration into a SiC powder remains poorly documented. Therefore, an investigation of a submicronic SiC powder dispersed in molten silicon is relevant. This is the purpose of this paper with the aim of providing a better understanding of the transformations occurring at micro- and macroscopic scales.

2. Materials and experimental procedures

A commercially available Si powder (99.995 wt.% Si, grade AX-20, Starck, Germany) was used in the experiments, with a mean particle size of 7.5 µm. The SiC powder (99.8 wt.%, Alfa Aesar, USA) contains 90% β-SiC and 10% α-SiC, with a particles size distribution characterized by d_{10} = 350 nm, d_{50}= 550 nm and d_{90} = 1000 nm (Fig. 1). SiC and Si powders were mixed and then compacted together with a volume ratio of 1:1 for a total mass of about 1g, the final porosity being of about 50%. The volume ratio was carefully selected because it promotes the solid-liquid interactions. This ratio is also suitable to prevent the collapse of the pellets and the gravitational sedimentation of SiC particles induced by an excess of molten silicon. The heating treatments of the pellets at 1450, 1500, 1550 and 1600°C were performed in an inductively heated graphite susceptor in the presence of hafnium powder as oxygen getter. A continuous flow of high purity argon under normal pressure was applied to prevent oxygen pollution. The temperature was increased rapidly (50°C.min^{-1}) up to the sintering temperature. The samples were then rapidly cooled (50°C.min^{-1}) at the end of heating. The determination of the crystallite sizes was performed by X-ray diffraction since it has been previously reported that this method is accurate up to crystallite sizes of about 100 nm or even 200 nm for a Cu-radiation [33-35]. Then, the samples were crunched to perform XRD experiments in Bragg-Brentano geometry with a Bruker D8 Advance diffractometer using a Cu Kα radiation fitted with a one-dimensional position sensitive silicon strip detector (Bruker, Linxeye). XRD patterns were recorded using a step size of 0.01° for a 2θ range of 20-140° and a counting time of 0.3 seconds per step. The freeware BRASS 2.0 was used for the profile fitting by Rietveld refinement including crystallite size calculations [36]. The instrumental broadening was defined using LaB_6 standard powder (NIST SRM660a). The zero shifts, roughness parameters, profile parameters, unit cell parameters, preferred orientation factor and isotropic temperature factors were refined in the Rietveld procedure using a pseudo-Voigt profile function. Atomic coordinates and site occupancies were however not refined since, in

all cases, no significant effect from internal microstrain was identified. The Lorentzian size and the Gaussian size were refined in order to provide apparent crystallite values. The quality of the fitting was estimated visually on the basis of the difference curve and by the R_{Bragg} factor which reaches values less than 5%. The microstructure of SiC grains was also analyzed by TEM (model 2100, JEOL).

3. Results and discussion

3.1 Crystallites growth

The size of SiC crystallites was estimated by Rietveld refinement from the X-ray diffraction patterns performed on 17 samples (Fig. 2) [37,38]. The value thus obtained is the radius corresponding to the equivalent spherical crystal noted *r*. The mean equivalent radius of the as-received powder was found close to 20±1 nm. Prior to the heat treatments of the mixed Si and SiC powders, pellets of only SiC powder was heated at 1550 and 1600°C during 6 hours. In this case, the equivalent crystal radius increase was low; the calculated values were found to be less than 30 nm with an incertitude of 5%. It was thus considered that within the 1450-1600°C range the crystal growth of isolated SiC powder was very weak. During heating between 1450 and 1600°C, the weight loss of silicon by evaporation after heating was lower than 5%, so that it could be considered that the remaining silicon was sufficient to promote a practically constant interaction with the powder. The mean equivalent crystal radii were measured by Rietveld refinements from X-ray diffraction experiments performed on crushed pellets. The results obtained thus are plotted in Figure 3-a). These plots indicate that an important crystal growth occurred during the first 60 minutes leading to *r* values of about 60 nm. The evolution of *r* strongly depends on the temperature; the highest value was measured close to 120 nm after a heating of 5 hours at 1600°C. An increase of the crystallites mean size during the heating is therefore confirmed. Theories of volume diffusion-controlled coarsening have been developed by Lifshitz, Slyozov [39] and Wagner [40] (LSW). In the LSW theory,

the growth of SiC crystallites or particles in liquid phase, called Ostwald ripening, is predicted to obey to Equation 1 [18]:

$$r^n - r_0^n = k(T).t \qquad \text{Equation 1}$$

with r being the radius of the particles after heating, r_0 the initial radius of the particles. *n* the Ostwald exponent generally comprised between 2 and 5. *k* is the kinetic coefficient of growth at a given temperature T and t the duration. The growth kinetics are controlled by the slower of the following two processes: 1) interface-reaction, which includes dissolution and precipitation; 2) diffusion. In any cases, the driving force for the dissolution of the smaller particles is their relatively high positive curvature which initiates a concentration gradient in the liquid phase. The rate-controlling mechanism is deduced from the rate-law exponent *n*. When the exponent *n* is equal to 2, the growth is controlled by interface-reaction. When *n* = 3, the growth is controlled by volume diffusion in the matrix, and for *n* = 4 the growth is limited by dissolution kinetics at the grain-matrix interface (boundary-diffusion controlled) [40-43]. The LSW theory assumes that the system is in a state of infinite dilution so that spherical particles cannot interact directly. In the present case, this assumption is invalid because (i) the volume fraction of the particles is 0.5 and (ii) the particles are not strictly spherical. However, various studies operating with low liquid fractions report a satisfying agreement with this theory, in spite of growth kinetics sometimes larger than the expected values [44,45]. According to the conclusions of H. Ye et al., it is considered that SiC coarsening mechanism is independent of the volume fraction of liquid provided that the liquid quantity is sufficient to cover each particle [22]. Consequently, the LSW theory is considered to be suitable in the present case as a thin liquid film is present between the particles. Indeed, the LSW theory is based on atoms transport by the liquid phase. The effect expected from a wide volume fraction of particles is first an acceleration of the coarsening kinetics because of the shorter average distance between particles. Then a decrease of the kinetics occurs due to the overlapping of the diffusion fields from closely-spaced neighboring particles. Indeed, it is worth noting that the diffusion fields from neighboring particles shall begin to overlap in a

much shorter time among closely-spaced particles with thin intervening liquid films than in thick liquid films. The linear regression corresponding to Equation 1 with *n* equal to 2, 3 and 4 are shown in Figure 3-b,c,d). The square relation is not convenient as the correlation coefficient R^2 is too low to be acceptable. The correlation coefficients of the cubic and fourth-power relations are close one to each other. Between these two solutions, the best correlation coefficient is obtained with the fourth powder law but this fact is not sufficiently convincing as the gap between the corresponding correlation coefficients R^2 is very weak. Indeed, it is comprised between 0.017 and 0.064. The fit to the fourth power relation is slightly better, especially for the highest temperature and duration as shown in Figure 3-d), which indicates that the growth is more probably controlled by dissolution of SiC in liquid silicon. The Arrhenius plot presented in Figure 4 was drawn for n = 3 and n = 4 on the basis of the corresponding law in the logarithmic form expressed by Equation 2:

$$Ln(k(T)) = Ln(k_0) - \frac{E_a}{R.T} \qquad \text{Equation 2}$$

where k_0 is a constant called frequency factor, E_a is the apparent activation energy, R is the gases constant and T is the absolute temperature. In both cases, a linear fit of the curve has been conclusively identified. The activation energies of the crystallites grow have been calculated from the slope of these curves and were found to be 357±50 kJ.mol^{-1} and 441±57 kJ.mol^{-1}, respectively for n = 3 and n = 4. This last value of the activation energy is consistent with the experimental dissociation energy of the Si-C bond which is reported to be equal to 451 kJ.mol^{-1}, which tends to confirm an interface-controlled reaction [46]. These energies are also lower than the ones reported by H. Schmidt at al. and R. Vaßen et al. in the absence of a liquid phase, which demonstrates the favorable effect of the liquid media on SiC ripening [31,32]. The existence of Ostwald ripening of SiC crystallites improved by molten silicon has then been confirmed and measured. Complementary TEM analyses were realized on the starting powder and on the sample heat treated at 1600°C for 5h, the corresponding brightfield (BF) of SiC grains being shown in Figures 5-a) and 5-c), respectively. On both pictures, one can see some large and faceted grains of about 1 µm. The selected area electron diffraction

(SAED) analyses of the SiC faceted grains marked as A and B are also shown in Figures 5-b) and 5-d), respectively. The indexing of the SAED patterns reveals that A and B are β-SiC crystals, which demonstrates the existence of large SiC crystals before and after the heating. Crystals larger than 200 nm have few or even negligible influences on the diffraction peaks broadening, so that Rietveld analysis method is not suitable for the measurement of such crystals [47]. This last method is particularly interesting as it highlights the presence of low-sized coherent domains corresponding to the highest chemical potentials and thus to the less thermodynamically stable fraction of the matter. Indeed, the high energies corresponding to the smallest crystallites constitute the driving force of the system's evolution to minimize this thermodynamic energy. The herein reported results confirm that, in spite of the presence of large crystals, the mean apparent crystallites size increases gradually with the duration of the heat treatments. One can state that small crystallites are always present it may be considered that their volume fraction decreases during the heating so that their effect on diffraction peaks broadening also decreases. The crystallites size measured from X ray diffraction experiments can also reveal various situations: the effective presence of nanometric-sized crystals and/or the presence of crystalline imperfections within wider crystals. Indeed, peaks broadening can also be induced by strain, atomic defects and interstitial atoms within crystalline networks which can also be progressively eliminated by thermal diffusion implying a decrease of the associated energy [48-51]. It is well known that such defects are relatively common in β-SiC [52-54] untill amorphization [55,56]. From our point of view, it would be more suitable to speak about apparent crystallites size. Furthermore, one has to underline that the smallness of the SiC crystallites implies the presence of numerous grain boundaries which can promote the mass transport and consequently the kinetics of crystallites growth. In the present case, the evolution of crystalline imperfections could influence the Ostwald exponent. Consequently, the definitive identification of the Ostwald exponent's value is made difficult because of possible fluctuations in time.

3.2 Particles coarsening

In order to estimate the variation of the size of SiC particles during the heat treatments, the Qin's method [57] was used by automatically drawing the circumference of each particle and determining the equivalent diameter of a circle of equal area with an *Image Analysis System* (*ImageJ*) [58]. The successive steps of an image analysis consist in adjusting the threshold for each image, setting the scale of the considered image and finally performing the analysis of the particles to obtain their surface and the equivalent diameter. The curve plot of the cumulative surface fraction versus the normalized diameters (d/d_{50}) is obtained by adding for each normalized diameter value the surface of the particles having at least the considered normalized diameter. Examples of micrographs thus obtained are given in Figure 6. Between 900 and 2100 polycrystalline particles were measured for each sample. Considering the resolution and the background noise of the micrographs used in this study, the minimum surface threshold was found equal to 40000 nm^2 corresponding to 16 neighboring pixels. The minimum equivalent diameter threshold of the measured particles is then equal to 200 nm. The boundaries between SiC particles appear to be sharp and generally easily distinguishable. Then, the evolution of the number of particles measured on the equivalent micrographs for each heat treatment is given in Figure 7. The frequency normalized to d_{50} and the cumulative surface fraction also normalized to d_{50} are presented in Figure 8. The corresponding d_{10}, d_{50}, d_{90}, and d_{max} values obtained from images analysis are given in Table 1, in which the considered number of particles are also indicated, the corresponding analyzed surfaces being similar. Considering the d_{50} increase during heating, an evolution towards larger values of the particles size distribution has been evidenced in many cases. For all the studied temperatures, the shape of the d/d_{50} distributions are close to the one of the starting powder, so that one can deduce that the particles growth evolves normally. The SEM micrographs in Figure 9 obtained from the starting powder and the longest heat treatments at 1450°C and 1600°C shows that some larger particles with arbitrary shapes have been generated, their proportion increasing slightly with time and duration but remaining very weak. As the surface fraction of

these particles is sufficiently noticeable, their presence is suitably evidenced by the sliding of the d_{50}-normalized cumulative surface fraction towards higher values. Therefore, six samples (1600°C/2;4;5h; 1550°C/0.5;1.5;6h) exhibit clearly larger d/d_{50} upper limits of the cumulative surface fraction than the one of the initial powder which is close to 4. The SEM micrograph of the sample heated at 1600°C for 0.5h shown in Figure 9-c) exhibits many large particles and a very reduced quantity of small ones. Some of these large particles appear to be faceted and thus probably monocrystalline, especially for the longest durations. The evolution of d_{10}, d_{50}, d_{90} and d_{max} of all samples are reported in Figure 10. The overall evolution follows a complex behavior depending on the temperature. As a matter of fact, the evolution of d_{10}, d_{50}, d_{90} and d_{max} follows three successive stages corresponding to (1) a fast increase, followed by (2) a decrease and then (3) a further increase. The first and second stages take place suddenly at 1550 and 1600°C, more slowly at 1500°C and appear to be very limited at 1450°C. Conversely, the lower is the temperature, the faster is the stage of final increase. There is yet some evidence that these results only give a partial appreciation of the particles size variations. Indeed, some additional points would be welcome especially close to the point of increase-decrease for a better delineation of this behavior shift. One has to note the correlation between the variation of the particles number and the d_{10}, d_{50} and d_{90} values, their variations being wholly inverted (Fig.7, Fig. 10). The analysis of the results indicates that the particles sizes vary in the lower durations with kinetics so elevated that they cannot be generated only by Ostwald ripening. The viscoplastic flow of SiC is considered as negligible because of the high covalent nature and low self-diffusivity which makes it very difficult to sinter to high density without sintering additives and pressure even at temperatures close to 2000°C. It was previously reported that the coarsening of dispersed particles in high volume fraction of liquid may occur by two different kinds of matter transport: by diffusion of chemical elements (Ostwald ripening), and by agglomeration-coalescence process generated by collisions between the particles leading to the formation of larger particles [59,60]. The agglomeration-coalescence proceeds by the contact of at least two particles with the absorption of the smaller

one by the larger one. The phenomenon of particles coarsening by collision in a liquid was examined by M. Smoluchowski [61] and H. Müller [62]. In the present case, one can deduce that such a phenomenon may occur at the same time as crystallites growth. This process is promoted by high-temperature convection movements of the liquid which enhances the particles 'mobility and therefore the contact between them and finally their agglomeration. This agglomeration phenomenon may occur with the presence of a transient thin film of the liquid between the grains. The fact that a decrease of the particles number is correlated to an increase of the particles size is coherent with SiC particles grouping. Moreover, the subsequent stage develops the increase of the particles number, which tends to demonstrate that the first growth of particles involves a reversible agglomeration process. The second increase of the d_{50} seems to follow a classic cubic law whereas the plot of the corresponding Arrhenius curve follows an almost linear variation (Fig. 11). The particularity, in this case, is the negative value of the apparent activation energy found approximately equal to -311 $kJ.mol^{-1}$. This highlights the fact that the higher kinetics of the second particles-size increase are measured at the lowest temperature. In others words, the growth mechanism of the mean particles is promoted by a lower temperature. This fact is unusual as growth mechanism by Ostwald ripening is thermally activated. The hypothesis of the simultaneous occurrence of several mechanisms thus appears to be relevant in the present case. On our point of view, the three mechanisms that could justify these observations are the agglomeration-coalescence, the fragmentation and the ripening. The agglomeration-coalescence and ripening processes lead respectively to a rapid and a slow increase of the size with a reduction of the particles number. Conversely, the fragmentation of the particles by collisions increase the particles number and decrease the mean size. This last phenomenon is the only one able to justify the size decrease. All the first rapid size increases are probably correlated to agglomeration-coalescence phenomenon that is the only one consistent with such elevated kinetics. The constant high ratio of small particles at the highest temperatures can be explained by collisions and ripening mechanisms that both generate continuously this type of particles.

3.3 Discussion

When considering the analyses of SiC crystallites and particles growth, it has been found that the growth of particles follows an unusual behavior that can be partly justified by the mobility of the particles in molten silicon. These identified variations thus identified are induced by the interfacial instability of the SiC grains. The Gibbs-Thomson effect, which formalizes the Ostwald ripening, can justify the general evolution of the grain sizes in a system where the phases are in equilibrium [63,64]. The driving force is generated by the very weak increase of the Gibbs energy at the surface of the grain correlated to the weakness of its radius. Considering the low radii of both the starting SiC particles and the apparent SiC crystallites, one can assume that the implied energies are substantial and consequently that they are at the origin of the herein experimental observations. We can consider that a global complex mechanism occurs which favors a putting in competition between several stabilization processes. One can suggest that the temperature tends at the same time to increase the instability of the system and its kinetics of evolution. In such a situation, the system tends to reduce as soon as possible its interface energy by the fastest stabilization process. Two processes of stabilization can be considered in the present case: the Ostwald ripening and the agglomeration-coalescence of the grains. The agglomeration-coalescence process promotes the minimization of the solid/liquid interface and consequently the corresponding energy. Its kinetic is relatively elevated, especially as the mobility of the particles increases with temperature. That is why this process is predominant at the highest temperatures, i.e. 1550 and 1600°C, leading to the relatively sudden formation of agglomerates. It also exists at 1500°C and probably also at 1450°C but in a weaker extent, the driving forces and the grains mobility being less favorable. Parallelly to the agglomeration-coalescence of the grains, a ripening also occurs which minimized the surface energy with lower kinetics as implying the temperature-activated diffusion coefficients of carbon atoms within SiC particles and Si melt. The decrease of the particles size at the highest temperatures is probably correlated to the

achievement of a critical radius, unstable to the interparticle collisions, and/or to the stabilization induced by ripening which, after generating a sufficient stabilizing effect, implies the breakdown of the agglomerates. Figure 12 proposes a schematic representation of this mechanism by considering two extreme cases corresponding to a low and a high temperature.

4. Conclusion

The Ostwald ripening of a submicronic SiC powder in the presence of molten silicon was examined during heating between 1450 and 1600°C. The increase of the crystallites size has been experimentally measured for the first time and the corresponding growth law was established. The activation energy was estimated to be equal to 357±50 $kJ.mol^{-1}$ or 441±57 $kJ.mol^{-1}$. The examination of the coarsening mechanism revealed a specific behavior which differs from the previously reported one. It could be proposed from the observations that SiC growth occurs by successive steps corresponding to the dissociation of less stable particles by dissolution in the liquid, the controlling process being mainly the dissolution of SiC in the liquid. It was also identified that an agglomeration-coarsening process occurs allowing the formation of larger polycrystalline particles. This behavior appears to be mainly temperature dependent. On the basis of these experimental results, it was shown that the interaction between a submicronic SiC powder and molten silicon is complex with at least two competitive processes: the apparent growth of SiC crystallites, fed by SiC dissolution, and the coarsening of SiC particles, driven by agglomeration. Nevertheless, the use of an adequate quantity of a liquid phase to facilitate the sintering of a nanocrystalline SiC powder seems to be an interesting way to produce SiC material at relatively low temperature and pressure, which should reduce the cost of such materials.

Acknowledgement

This work has been performed within the frame of the training stay of J. Poinsot from PHELMA Grenoble.

The authors wish to thank Dr. Julien Danet, from the Laboratory of ThermoStructural Composites, for his assistance in TEM analysis.

References

[1] R. W. Bartlett, W. E. Nelson, F. A. Halden, Influence of carbon transport kinetics on solution growth of 3C-silicon carbide crystals, J. Electrochem. Soc. 11 (1967) 1149-1154.

[2] R. Deike, K. Schwerdlfeger, Reactions between liquid silicon and different refractory materials, J. Electrochem. Soc. 142(2) (1995) 609-614.

[3] R. Pampuch, E. Walasek, J. Bialoskbrski, Reaction mechanism in carbon-liquid silicon systems at elevated temperatures, Ceram. Inter. 12 (1986) 99-106.

[4] H. Zhou, R.N. Singh, Kinetics model for the growth of silicon carbide by reaction of liquid silicon with carbon, J. Am. Ceram. Soc. 78(9) (1995) 2456-2462.

[5] J.G. Li, H. Hausner, Reactive wetting in the liquid-silicon/solid-carbon system, J. Am. Ceram. Soc. 79(4) (1996) 873-880.

[6] V. Bougiouri, R. Voytovych, N. Rojo-Calderon, J. Narciso, N. Eustathopoulos, The role of the chemical reaction in the infiltration of porous carbon by NiSi alloys, Scr. Mater. 54 (2006) 1875-1878.

[7] R. Pampuch, J. Bialoskbrski, E. Walasek, Mechanism of reactions in the $Si_l + C_f$ system and the self-propagating high-temperature synthesis of silicon carbide, Ceram. Inter. 13 (1987) 63-68.

[8] A. Favre, H. Fuzellier, An original way to investigate the siliconizing of carbon materials, J. Suptil, Ceram. Inter. 29 (2003) 235-243.

[9] O.P. Chakrabarti, P.K. Das, J. Mukerji, Growth of SiC particles in reaction sintered SiC, Mater. Chem. Phys. 67 (2001) 199.

[10] J.C. Margiotta, D. Zhang, D.C. Nagle, C.E. Feeser, Formation of dense silicon carbide by liquid silicon infiltration of carbon with engineered structure, J. Mater. Res. 23(5) (2008) 1237-1248.

[11] W.E. Lee, D.D. Jayaseelan, S. Zhang, Solid–liquid interactions: The key to microstructural evolution in ceramics, J. Eur. Ceram. Soc. 28 (2008) 1517-1525.

[12] M. Keppeler, H.-G. Reichert, J. M. Broadley, G. Thurn, I. Wiedmann, F. Aldinger, High temperature mechanical behaviour of liquid phase sintered silicon carbide, J. Eur. Ceram. Soc. 18 (1998) 521-526.

[13] J. Wang, W. Lin, Z. Jiang, L. Duan, G. Yang, The preparation and properties of SiCw/B_4C composites infiltrated with molten silicon, Ceram. Inter. 40 (2014) 6793-6798

[14] C. Zhang, H. Ru, H. Zong, W. Sun, J. Zhu, W. Wang, X. Yue, Coarsening of boron carbide grains during the infiltration of porous boron carbide preforms by molten silicon, Ceram. Inter. 42 (2016) 18681-18691.

[15] S. Song, C. Bao, Y. Ma, K. Wang, Fabrication and characterization of a new-style structure capillary channel in reaction bonded silicon carbide composites, J. Eur. Ceram. Soc. 37 (2017) 2569-2574

[16] Y.W. Kim, M. Mitomo, G.D. Zhan, Mechanism of grain growth in liquid-phase-sintered β–SiC, J. Mater. Res. 14(11) (1999) 4291-4293.

[17] W. Ostwald, Analytische Chemie, third ed., Engelmann, Leipzig, 1901.

[18] R.D. Vengrenovitch, On the Ostwald ripening theory, Acta Metall. 30 (1982) 1079-1086.

[19] J.H. Yao, K.R. Elder, H. Guo, M. Grant, Theory and simulation of Ostwald ripening, Phys. Rev. B 47(21) (1993) 14110-14125.

[20] H. Fischmeister, G. Grimvall, in: G.C. Kuczynski (Eds.), Sintering and related Phenomena, Springer US, 1973, pp. 119-149.

[21] L.S. Sigl, H.J. Kleebe, Core/Rim Structure of Liquid-Phase-Sintered Silicon Carbide, J. Am. Ceram. Soc. 76 (1993) 773-776.

[22] H. Ye, V.V. Pujar, N.P. Padture, Coarsening in liquid-phase-sintered α-SiC, Acta Mater. 47 (1999) 481-487.

[23] M.S. Datta A.K. Bandyopadhyay, B. Chaudhuri, Sintering of nano crystalline α silicon carbide by doping with boron carbide, Bull. Mater. Sci. 25 (2002) 181-189.

[24] A. Swiderska-Sroda, G. Kalisz, B. Palosz, N. Herlin-Boime, SiC Nano-ceramics sintered under high-pressure, Rev. Adv. Mater. Sci. 18 (2008) 422-424.

[25] X. Mao-lin, L. De-li, X. Xiao-bin, L. Bang-yi, C. Chang'an, L. Wei-yuan, Densification of nano-SiC by ultra-high-pressure effects of time, temperature, and pressure, Fusion Eng. Des. 85 (2010) 964-968.

[26] A. Malinge, A. Coupé, Y. Le Petitcorps, R. Pailler, Pressureless sintering of beta silicon carbide nanoparticles, J. Eur. Ceram. Soc. 32 (2012) 4393-4400.

[27] F. Lomello, G. Bonnefont, Y. Leconte, N. Herlin-Boime, G. Fantozzi, Processing of nano-SiC ceramics: Densification by SPS and mechanical characterization, J. Eur. Ceram. Soc. 32 (2012) 633-641.

[28] M. Hotta, J. Hojo, Effect of AlN additive on densification, microstructure and strength of liquid-phase sintered SiC ceramics by spark plasma sintering, J Ceram. Soc. Jpn. 117 (2009) 1009-1012.

[29] M. Mitomo, Y-W Kim, H.Hirotsuru, Fabrication of silicon carbide nanoceramics. J Mater. Res. 11 (1996) 1601-1604.

[30] X. Zhou, J. Zang, L. Dong, X. Cheng, T. Li, Y. Wang, Y. Yuan, J. Lu, Y. Yu, X. Xu, Fabrication of bulk nano-SiC via in-situ reaction of core-shell structural SiC-C with Si using high pressure high temperature sintering method, Mater. Lett. 144 (2015) 69-73.

[31] H. Schmidt, W. Gruber, G. Borchardt, P. Gerstel, A. Muller, N. Bunjes, Coarsening of nano-crystalline SiC in amorphous Si–B–C–N, J. Eur. Ceram. Soc. 25 (2005) 227-231.

[32] R. Vaßen, A. Kaiser, J. Forster, H.P. Buchkremer, D. Stover, Densification of ultrafine SiC powders, J. Mater. Sci. 31 (1996) 3623-3637

[33] Weibel A, Bouchet R, Boulc'h F, Knauth P. The big problem of small particles: a comparison of methods for determination of particle size in nanocrystalline anatase powders, Chem. Mater. 17 (2005) 2378-2385.

[34] R. Guinebretière, X-ray diffraction by polycrystalline materials, John Wiley & Sons, London, 2007.

[35] A. Guinuer, X-ray diffraction in crystals, imperfect crystals, and amorphous bodies. Dover Publications Inc., New York, 1994.

[36] J. Birkenstock, R.X. Fischer, T. Messner, (2004), BRASS 2, the Bremen Rietveld Analysis and Structure Suite, University of Bremen.

[37] H.M. Rietveld, A profile refinement method for nuclear and magnetic structures, J. Appl. Crystallogr. 2 (1969) 65-71.

[38] J. Rodriguez-Carvajal, Recent advances in magnetic structure determination by neutron powder diffraction, Physica B 192 (1993) 55-69.

[39] I.M. Lifshitz, V.V. Slyozov, The kinetics of precipitation from supersaturated solid solutions, J. Phys. Chem. Solids 19 (1961) 35-50.

[40] C.Z. Wagner, Theorie der Alterung von Niederschlägen durch Umlösen (Ostwald-Reifung), Elektrochem. 65 (1961) 581-591.

[41] H.O.K. Kirchner, Coarsening of grain-boundary precipitates, Metall. Trans. 2 (1971) 2861-2864.

[42] M.V. Speight, Growth kinetics of grain-boundary precipitates, Acta Metall. 16 (1968) 133-135.

[43] D. Hu, M.H. Loretto, Coarsening of TiC particles in a rapidly solidified Ti6Al4V-TiC composite, J. Alloys Compds. 209 (1994) 167-173.

[44] S.C. Hardy, P.W. Voorhees, Ostwald ripening in a system with a high-volume fraction of coarsening phase, Metall. Mater. Trans. 19A (1988) 2713-2721.

[45] V.A. Snyder, J. Alkemper, P.W. Voorhees, Transient Ostwald ripening and the disagreement between steady-state coarsening theory and experiment, Acta Mater. 49 (2001) 699-709.

[46] D.R. Lide, CRC Handbook of Chemistry and Physics, 95th ed., CRC Press, Boca Raton, 2014.

[47] V. Uvarov, I. Popov, Metrological characterization of X-ray diffraction methods at different acquisition geometries for determination of crystallite size in nano-scale materials, Mater. Charact. 85 (2013) 111-123.

[48] E. Wu, E. Mac A. Gray, E. H. Kisi, Modelling Dislocation-lnduced Anisotropic Line Broadening in Rietveld Refinements Using a Voigt Function. I. General Principles, J. Appl. Cryst. 31 (1998) 356-362.

[49] J. Chrosch, M. Colombo, I. Memmi, R. Biagini, Defect-induced microstructures an X-ray diffraction analysis, J. Mater. Sci. 34 (1999) 2263-2267.

[50] T. Ungaar, J. Gubicza, G. Ribaarik and A. Borbealy, Crystallite size distribution and dislocation structure determined by diffraction profile analysis: principles and practical application to cubic and hexagonal crystals, J. Appl. Cryst. 34 (2001) 298-310.

[51] T. Ungar, Microstructural parameters from X-ray diffraction peak broadening, Scripta Mater. 51 (2004) 777-781.

[52] A. Zywietz, J. Furthmuller, F. Bechstedt, Vacancies in SiC: Influence of Jahn-Teller distortions, spin effects, and crystal structure, Phys. Rev. B 59(23) (1999) 15166-15180.

[53] M. Dudley, X.R. Huang, W.M. Vetter, Contribution of x-ray topography and high-resolution diffraction to the study of defects in SiC, J. Phys. D: Appl. Phys. 36 (2003) A30-A36.

[54] J. Xi, B. Liu, Y. Zhang, W.J. Weber, Ab initio study of point defects near stacking faults in 3C-SiC, Comput. Mater. Sci. 123 (2016) 131-138.

[55] A. Boulle, A. Debelle, J.B. Wallace, L.B. Bayu Aji, S.O. Kucheyev, The amorphization of 3C-SiC irradiated at moderately elevated temperatures as revealed by X-ray diffraction, Acta Mater. 140 (2017) 250-257.

[56] D.J. Sprouster, T. Koyanagi, E. Dooryhee, S.K. Ghose, Y. Katoh, L.E. Ecker, Reprint of: Microstructural evolution of neutron irradiated 3C-SiC, Scr. Mater. 143 (2018) 176-180.

[57] Y. Qin, G. Götz, W. Blum, Z.G. Zhu, Determination of size distribution of precipitates in the cast martensitic steel G-X12CrMoWVNbN 10-1-1 by direct and indirect method, J. Alloys Compds. 352 (2003) 260-264.

[58] C.A. Schneider, W.S. Rasband, K.W. Eliceiri, NIH Image to ImageJ: 25 years of image analysis, Nature methods 9 (2012) 671-675.

[59] L. Ratke, Simultaneous coarsening of dispersions by growth and coagulation, J. Colloid Interface Sci. 119 (1987) 391-397.

[60] H. E. Exner, E. Arzt, "Physical Metallurgy", R. W. Cahn and P. Haasen Eds., Vol. II, Amsterdam, 1984.

[61] M. Smoluchowski, Drei vortrage uber Diffusion. Brownsche Bewegung und Koagulation von Kolloidteilchen, Phys. Z. 17 (1916) 585-599.

[62] H. Müller, Zur allgemeinen Theorie ser raschen Koagulation, Kolloidchem. Beih. 27 (1928) 223-250.

[63] J.J. Thomson, Applications of dynamics to physics and chemistry, Macmillan & Co., Londres, 1888.

[64] W. Ostwald, Analytische Chemie, 3rd edition, Engelmann, Leipzig, 1901.

Table 1: Results of the image analysis with *ImageJ* software for the starting powder (0h on the 1550°C line) and after heat treatments at 1450, 1500, 1550 and 1600°C for various durations.

1450°C	**1h**	**2h**	**3h**	**5h**	**8h**
d_{10} **(µm)**	0.29	0.30	0.31	0.36	0.40
d_{50} **(µm)**	0.65	0.70	0.71	0.81	0.89
d_{90} **(µm)**	1.31	1.39	1.40	1.64	1.74
d_{max} **(µm)**	3.45	3.84	3.98	3.46	3.81
Particles number	1843	1811	1796	1335	1247
1500°C	**0.5h**	**1h**	**2h**	**4h**	**8h**
d_{10} **(µm)**	0.32	0.32	0.32	0.35	0.39
d_{50} **(µm)**	0.74	0.72	0.75	0.77	0.81
d_{90} **(µm)**	1.47	1.42	1.41	1.51	1.61
d_{max} **(µm)**	2.99	4.00	3.55	3.51	3.82
Particles number	1671	1749	1539	1536	1431
1550°C	**0h**	**0.25h**	**0.5h**	**1.5h**	**6h**
d_{10} **(µm)**	0.27	0.38	0.39	0.31	0.34
d_{50} **(µm)**	0.62	0.89	0.80	0.77	0.82
d_{90} **(µm)**	1.19	1.94	1.65	1.65	1.69
d_{max} **(µm)**	2.98	3.26	4.54	3.92	3.98
Particles number	2122	903	1452	1382	1283
1600°C	**0.25h**	**0.5h**	**2h**	**4h**	**5h**
d_{10} **(µm)**	0.44	0.49	0.30	0.33	0.34
d_{50} **(µm)**	0.87	0.94	0.73	0.74	0.75
d_{90} **(µm)**	1.72	1.77	1.67	1.67	1.64
d_{max} **(µm)**	4.28	3.60	4.61	6.82	4.43
Particles number	1162	1347	1302	1123	1359

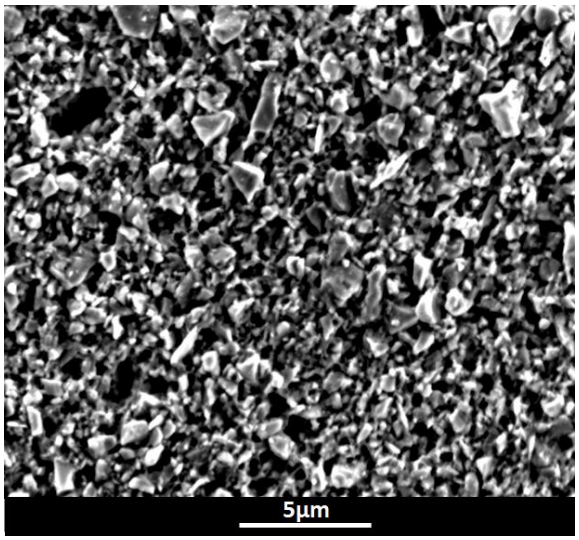

Figure 1. SEM image of the starting SiC powder

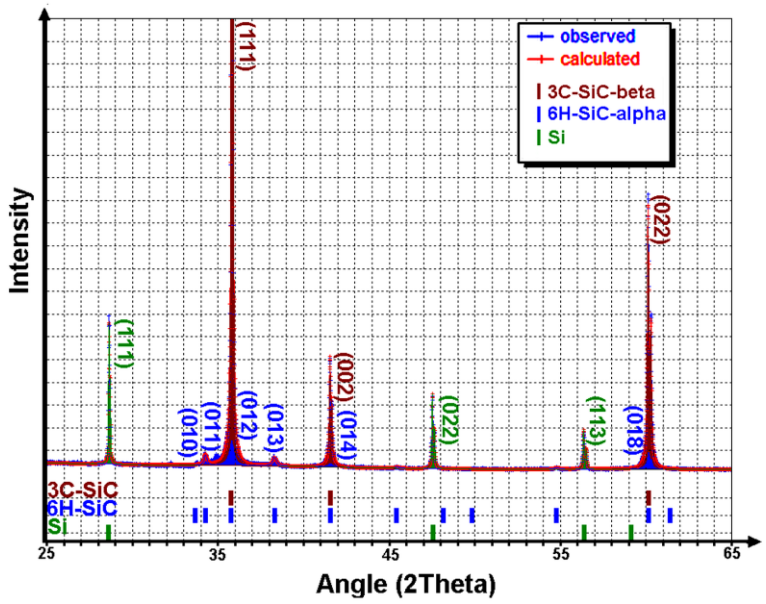

Figure 2. X-ray diffraction pattern and phases indexation of the SiC/Si sample heat treated at 1450°C for 8 hours

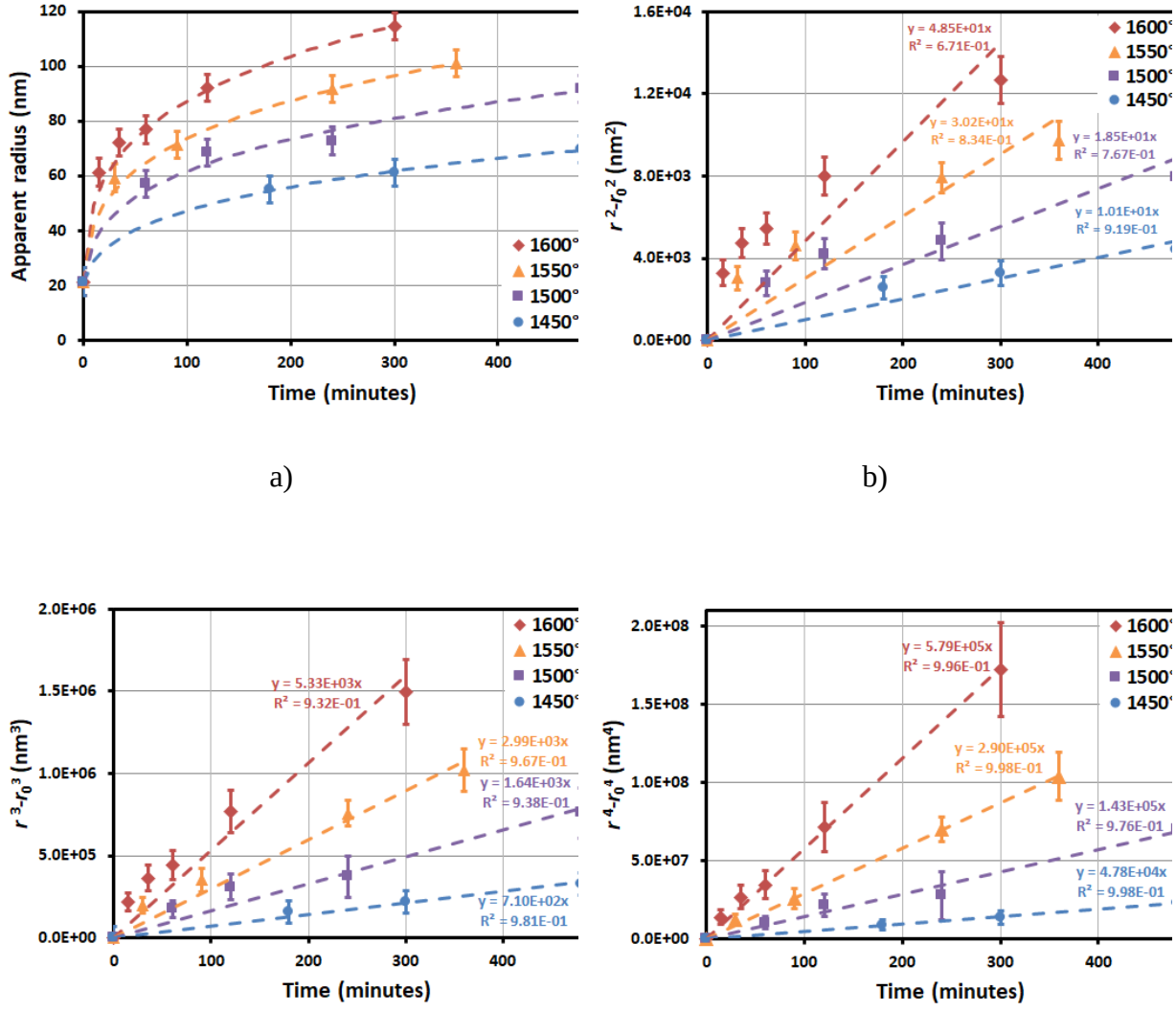

Figure 3. Evolution of the SiC crystallites mean radius in the SiC/Si mixtures heat treated between 1450 and 1600°C showing: a) the dependency of the radius on time, and b), c), d) the variations of the radius plotted as function of the various laws r^2-r_0^2=f (t), r^3-r_0^3=f (t) and r^4-r_0^4=f (t) with the corresponding linear fits (dotted lines).

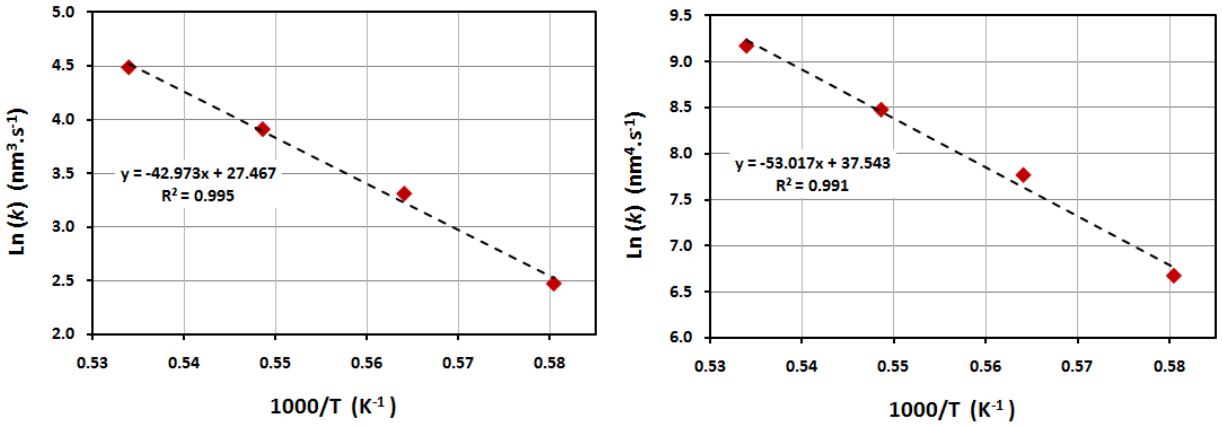

a) b)

Figure 4. Arrhenius plot Ln(k) = f (1000/T) of the SiC crystal growth between 1450 and 1600°C for: a) n = 3 and b) n = 4. The dotted lines are the linear fits.

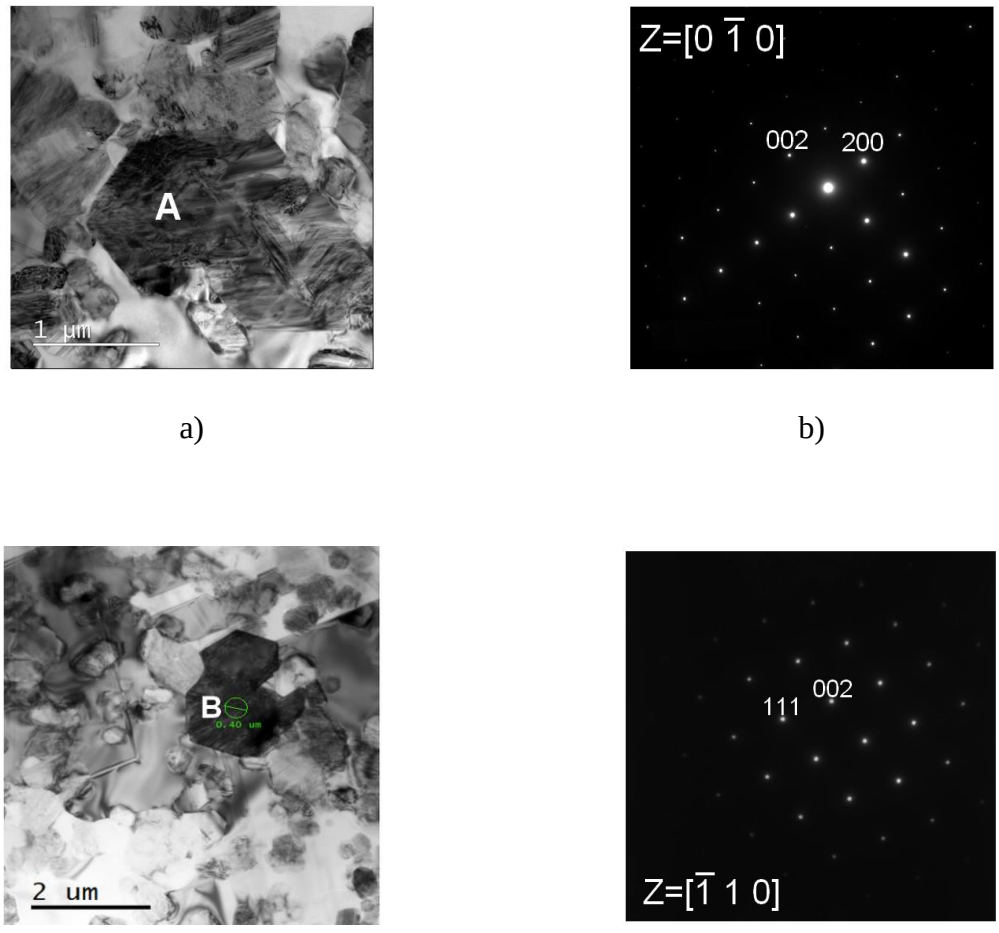

a) b)

c) d)

Figure 5. TEM analysis of β-SiC grains: a) BF on the so-received powder, b) SAED of a grain of the starting powder, c) BF of the sample heated at 1600°C/5h, d) SAED of a grain of the

sample heated at 1600°C/5h.

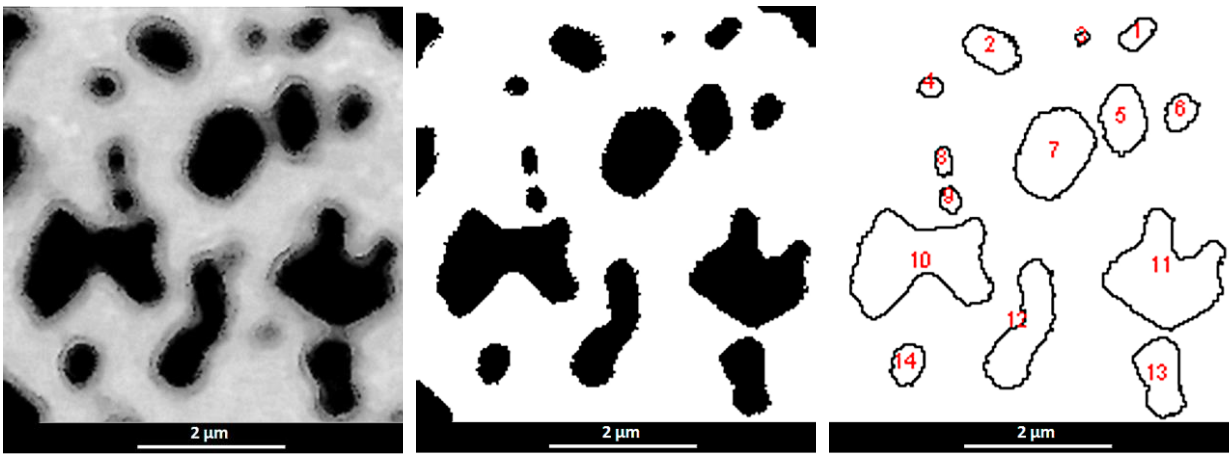

a) b) c)

Figure 6. Schematic diagrams of the process used to determine the size and distribution of particles: a) SEM image of SiC particles, b) particle separation using an image processing software, c) profiles and numbering of particles after size determination using *Image J* [58].

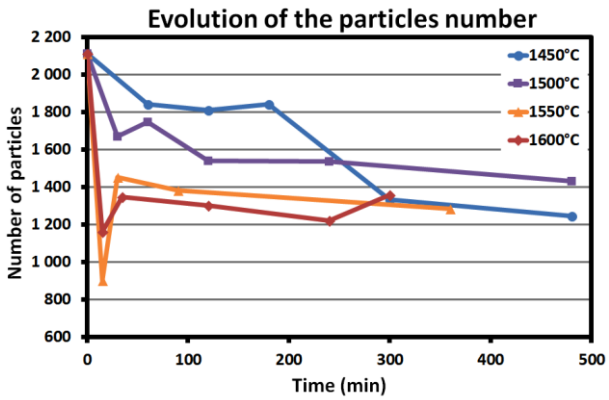

Figure 7. Evolution of the number of particles number during the heat treatments performed at 1450, 1500, 1550 and 1600°C as a function of durations.

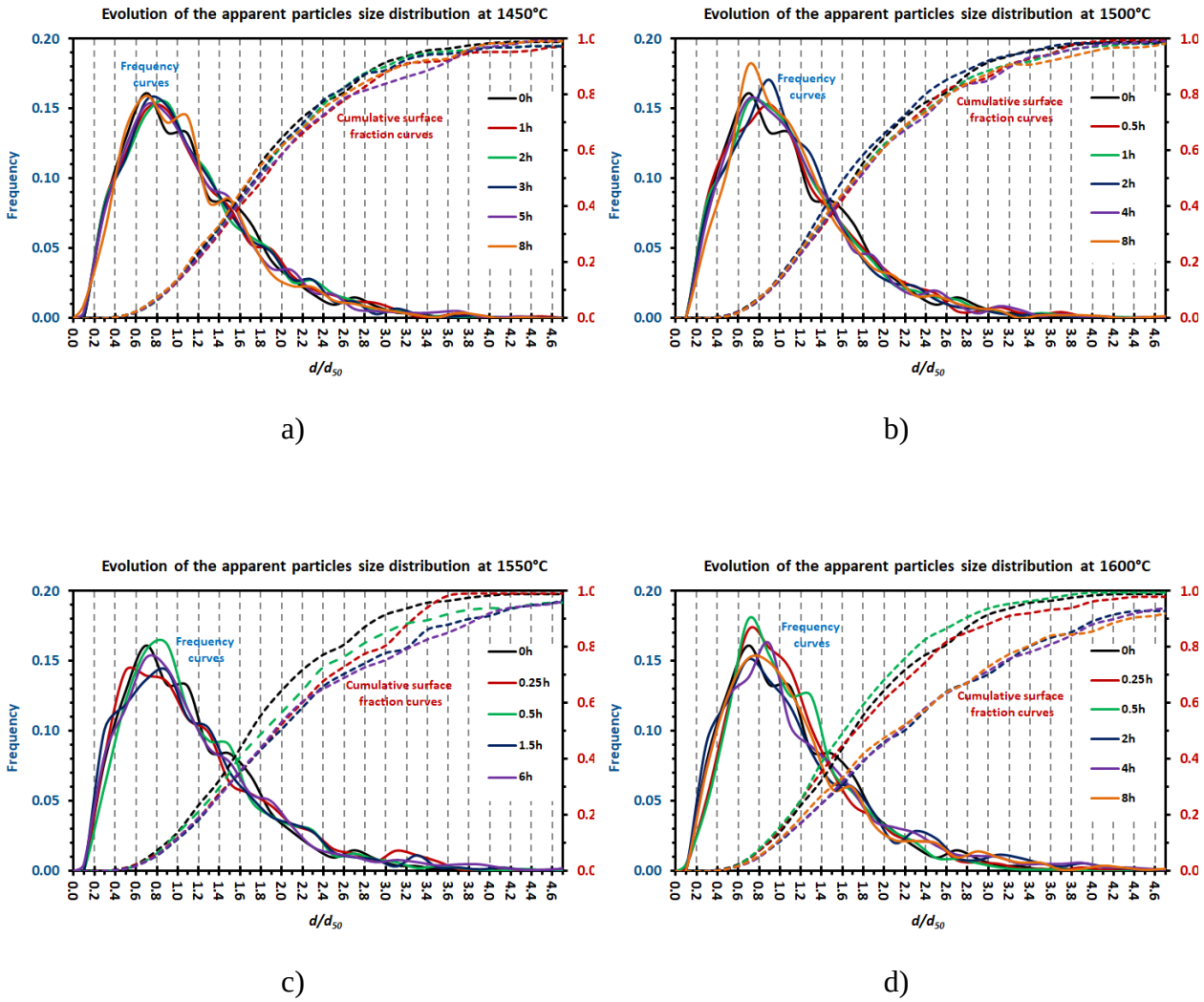

Figure 8. SiC particles distributions of the starting powder and after heating at: a) 1450°C, b) 1500°C, c) 1550°C; and d) 1600°C for various durations.

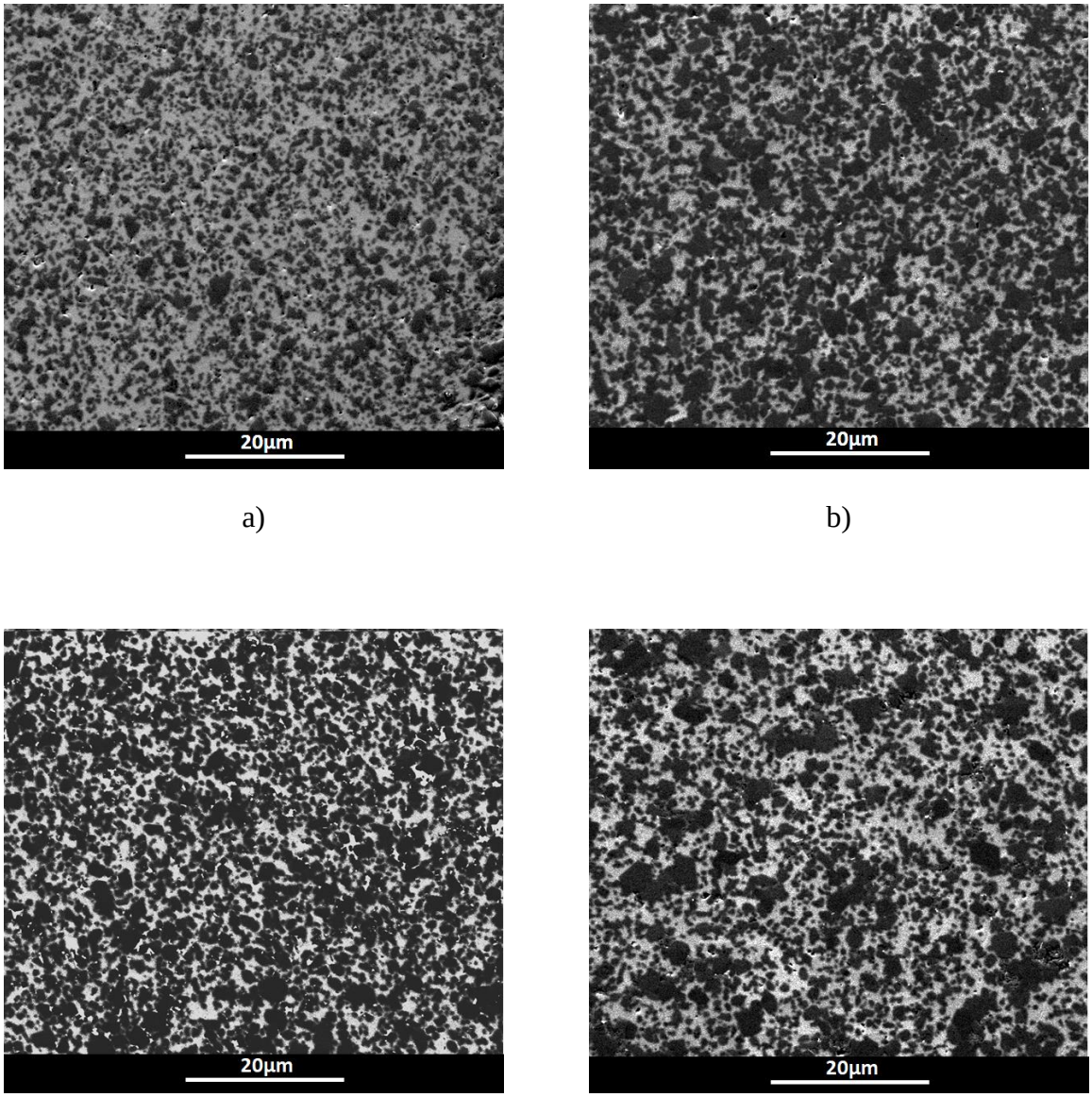

a) b)

c) d)

Figure 9. Backscattered electrons images of: (a) the starting sample $SiC_{50vol.\%}+Si_{50vol.\%}$, and after heating: (b) 1450°C for 8h, (c) 1600°C for 0.5h; and (d) 1600°C for 5h.

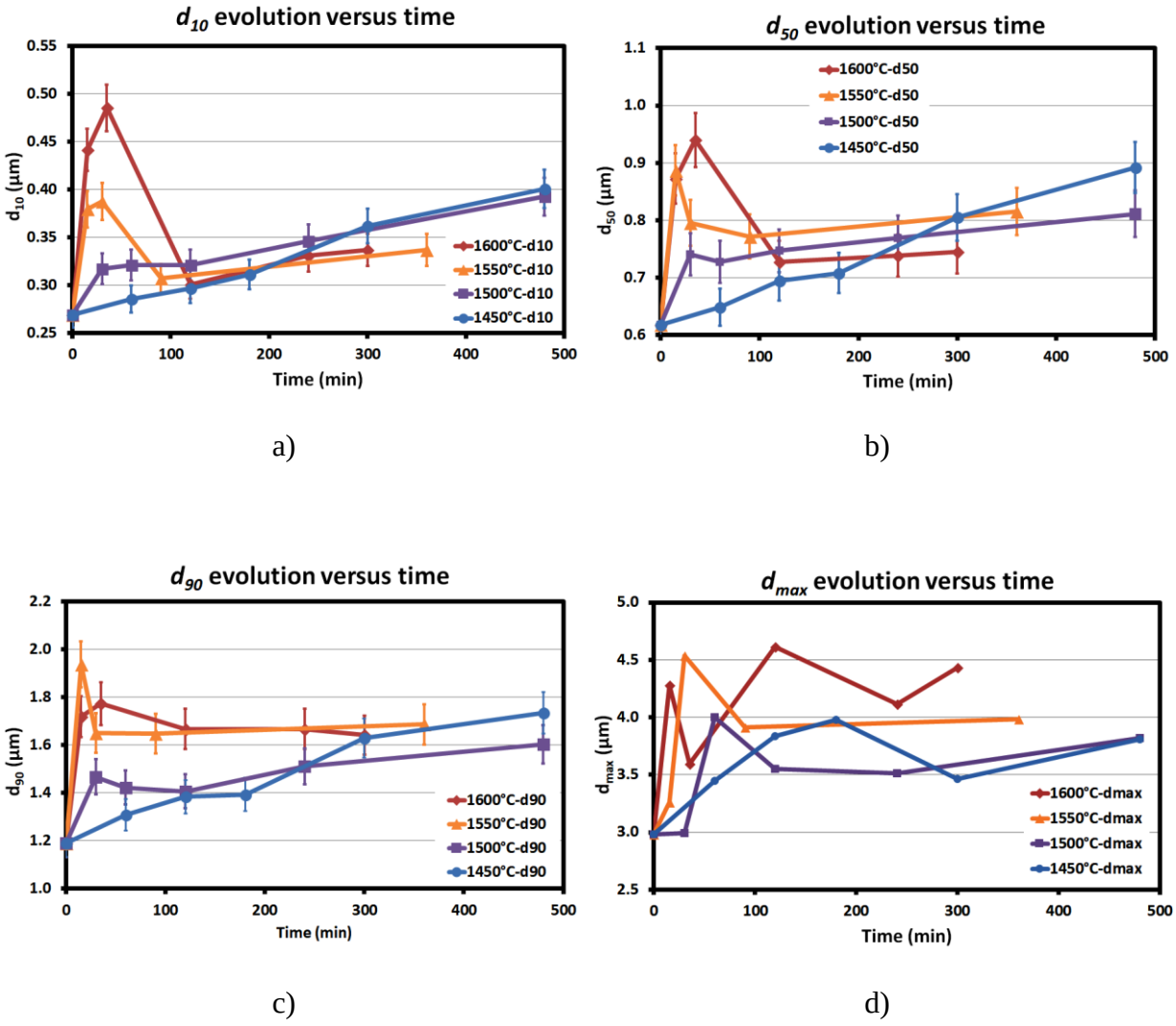

Figure 10. Evolution of the size of the particles during heating at 1600°C and 1450°C: a) d_{10}, b) d_{50}, c) d_{90}; and d) d_{max}.

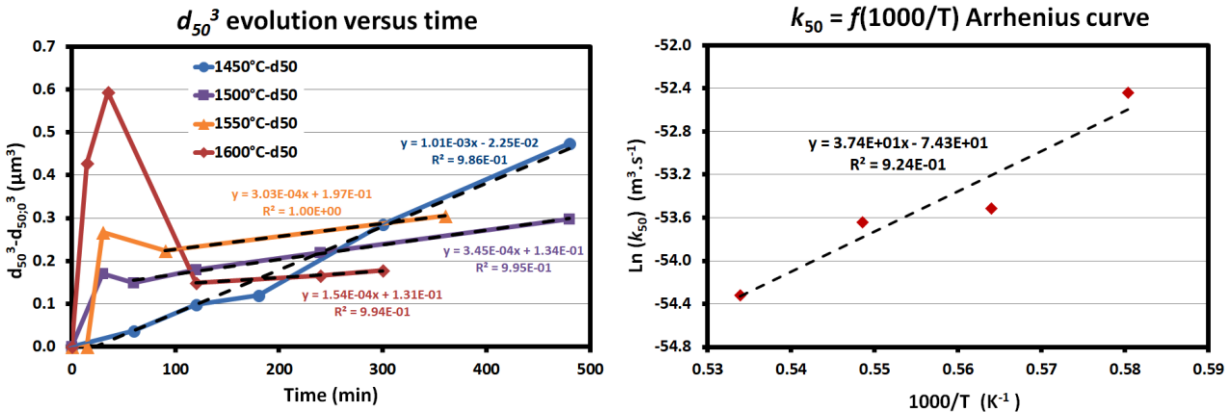

a) b)

Figure 11. d_{50} evolution of the SiC particles during heating: a) d_{50}^3- $d_{50;0}^3$ as a function of the duration of heating; and b) k_{50} Arrhenius curve.

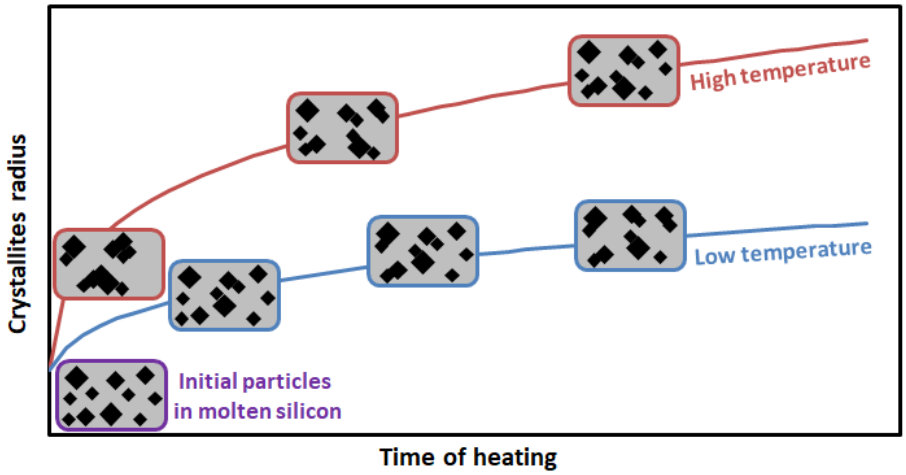

Figure 12. Schematic representation of the mechanism of the SiC evolution in molten silicon at low and high temperatures: increase of the average crystallites radius and variation of the particles size